Focused Blind Deconvolution

Pawan Bharadwaj [iD], Laurent Demanet [iD], and Aimé Fournier

Abstract—We introduce a novel multichannel blind deconvolution (BD) method that extracts *sparse* and *front-loaded* impulse responses from the channel outputs, i.e., their convolutions with a single arbitrary source. Unlike most prior work on BD, a crucial feature of this formulation is that it does not encode support restrictions on the unknowns, except for fixing their duration lengths. The indeterminacy inherent to BD, which is difficult to resolve with a traditional ℓ_1 penalty on the impulse responses, is resolved in our method because it seeks a first approximation where the impulse responses are: "maximally white" over frequency—encoded as the energy focusing near zero lag of the impulse-response temporal autocorrelations; and "maximally front-loaded"—encoded as the energy focusing near zero time of the impulse responses. Hence, we call the method focused BD (FBD). It partitions BD into two separate optimization problems and uses the focusing constraints in succession. The respective constraints in both these problems are removed as the iterations progress. A multichannel BD problem whose physics calls for sparse and front-loaded impulse responses arises in seismic inversion, where the impulse responses are the Green's function evaluations at different receiver locations, and the operation of a drill bit inputs the noisy and correlated source signature into the subsurface. We demonstrate the benefits of FBD using seismic-while-drilling numerical experiments, where the noisy data recorded at the receivers are hard to interpret, but FBD can provide the processing essential to separate the drill-bit (source) signature from the interpretable Green's function.

Index Terms—Blind deconvolution, seismic interferometry, phase retrieval, channel identification, dereverberation, front-loaded, coprime.

I. INTRODUCTION

THERE are situations where seismic experiments are to be performed in environments with a noisy source e.g., when an operating borehole drill is loud enough to reach the receivers in the borehole or on the surface. The source generates an unknown, noisy signature $s(t)$ at time t; one typically fails to dependably extract the source signature despite deploying an attached receiver. For example, the exact signature of the operating drill bit in a borehole environment cannot be recorded because there would always be some material interceding before the receiver [1]. The noisy-source signals propagate through

the subsurface, and result in the data at the receivers, denoted by $d_i(t)$ at receiver i. Imaging of the data to characterize the subsurface (seismic inversion) is only possible when they are deconvolved to discover the subsurface Green's function. Similarly, in room acoustics, the speech signals $s(t)$ recorded as $d_i(t)$ at a microphone array are distorted and sound reverberated due to the reflection of walls, furniture and other objects. Speech recognition and compression is simpler when the reverberated records $d_i(t)$ at the microphones are deconvolved to recover the clean speech signal [2], [3].

The response of many such physical systems to a noisy source is to produce multichannel outputs. The n observations or channel outputs, in the noiseless case, are modeled as the output of a linear system that convolves (denoted by $*$) a source (with signature $s(t)$) with the impulse response function:

$$d_i(t) = \{s * g_i\}(t). \tag{1}$$

Here, $g_i(t)$ is the ith channel impulse response and $d_i(t)$ is the ith channel output. The impulse responses contain physically meaningful information about the channels. Towards the goal of extracting the vector of impulse responses $[g_1(t), \ldots, g_n(t)]$ or simply $[g_i]$ and the source function $s(t)$, we consider an unregularized least-squares fitting of the channel-output vector $[d_1(t), \ldots, d_n(t)]$ or $[d_i]$. This corresponds to the least-squares multichannel deconvolution [4]–[6] of the channel outputs with an unknown blurring kernel i.e., the source signature. It is well known that severe non-uniqueness issues are inherent to multichannel blind deconvolution (BD); there could be many possible estimates of $[g_i]$, which when convolved with the corresponding s will result in the recorded $[d_i]$ (as formulated in (6) below).

Therefore, in this paper, we add two additional constraints to the BD framework that seek a solution where $[g_i]$ is:

1) *maximally white* — encoded as the energy focusing near zero lag (i.e., energy diminishing at non-zero lags) of the impulse-response auto-correlations and
2) *maximally front-loaded* — encoded as the energy focusing near zero time of the most front-loaded impulse response.

We refer to them as *focusing* constraints. They are not equivalent to ℓ_1 minimization,[1] although they also enforce a form of sparsity. These are relaxed as the iterations progress to enhance the fitting of the channel outputs. Focused blind deconvolution (FBD) employs the focusing constraints to resolve the indeterminacy inherent to the BD problem. We identify that it is more favorable to use the constraints in succession after decomposing the BD problem into two separate least-squares optimization problems. The first problem, where it is sufficient to employ the

---

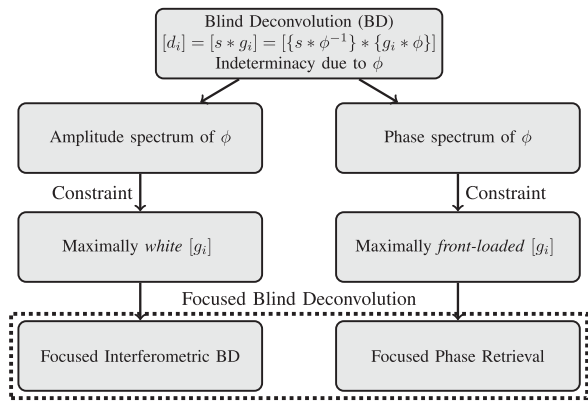[1]That is, minimizing $\sum_t |g_i(t)|$ to promote sparsity.

Fig. 1. Focused blind deconvolution uses two focusing constraints to resolve the indeterminacies of the multichannel blind deconvolution. Note that this is not an algorithmic flowchart, but explains the two components of the regularization in FBD.

first constraint, fits the *interferometric or cross-correlated* channel outputs [7], rather than the raw outputs, and solves for the interferometric impulse response. The second problem relies on the outcome of the previous problem and completes FBD by employing the second constraint and solving for the impulse responses from their cross-correlations. This is shown in the Fig. 1. According to our numerical experiments, FBD can effectively retrieve $[g_i]$ provided the following conditions are met:

1) the duration length of the channel outputs should be long enough to contain the unknown impulse responses;
2) the channels are *sufficiently dissimilar* in the sense of their transfer-function polynomials being *coprime* in the z-domain (to be elucidated below).

In the seismic inversion context, an approximate duration length of the unknown impulse responses can be easily determined (see Section V) by utilizing the source and receiver locations. The first condition is economically beneficial , as usual drilling practice enables experiments to record noisy data for a time period much longer compared to the wave-propagation time. Also, since drilling is anyway necessary, its use as a signal source to estimate $[g_i]$ is a free side benefit. We show that the second condition can be satisfied in the seismic experiments by deploying *sufficiently dissimilar* receivers, as defined below, which may yet be arrayed variously in a borehole, or surface-seismic geometry.

It is shown in [8] that multichannel blind deconvolution is dependent on the condition that the transfer functions are coprime i.e., they do not share common roots in the z-domain. The BD algorithms in [9], [10] are also based on this prerequisite. In this regard, due to the difficulty of factoring the high order channel polynomials, [11] proposed a method for identification of common roots of two channel polynomials. Interestingly, they have observed that the roots do not have to be exactly equal to be considered common in BD. Khong *et al.* [12] uses clustering to efficiently extract clusters of near-common roots. In contrast to these methods, FBD doesn't need the identification of the common roots of the channel polynomials.

Surveys of BD algorithms in the signal and image processing literature are given in [13], [14]. A series of results on blind

deconvolution appeared in the literature using different sets of assumptions on the unknowns. The authors in [15], [16] show that BD can be efficiently solved under certain subspace conditions on both the source signature and impulse response even in a single-channel case. The recovery of the unknowns in multichannel BD assuming that the source is sparse in some known basis and the impulse responses belong to known random subspaces is shown by [17]. The experimental results in [18] show the successful joint recovery of Gaussian impulse responses with known support that are convolved with a single Gaussian source signature. BD algorithms with various assumptions on input statistics are proposed in [19]–[21]. Compared to the work in these articles, FBD doesn't require any assumptions on

1) support of the unknowns,
2) statistics of the source signature and
3) the underlying physical models;[2]

although, it does apply a type of sparsity prior on $[g_i]$. Note also that regularization in the sense of minimal ℓ_1 i.e., mean-absolute norm, as some methods employ, does not fully address the type of indeterminacy associated with BD — we have clarified this in appendix A. Recent work in [24], [25] conducts geometric analysis of such sparse blind deconvolution methods by employing an additional constraint that the source has unit ℓ_2 norm.

Deconvolution is also an important step in the processing workflow used by exploration geophysicists to improve the resolution of the seismic records [26]–[28]. Robinson [29] developed predictive decomposition [30] of the seismic record into a source signature and a white or uncorrelated time sequence corresponding to the Earth's impulse response. In this context, the elements of $[g_i]$ correspond to the unique subsurface Green's function $g(\vec{x}, t)$ evaluated at the receiver locations in $[\vec{x}_i]$, where the seismic-source signals are recorded. Here $\vec{x}$ denotes a vector of spatial coordinates. Spiking deconvolution [31], [32] estimates a Wiener filter that increases the *whiteness* of the seismic records, therefore, removing the effect of the seismic sources. In order to alleviate the non-uniqueness issues in blind deconvolution, recent algorithms in geophysics:

1) take advantage of the multichannel nature of the seismic data [33]–[36];
2) sensibly choose the initial estimate of $[g_i]$ in order to converge to a desired solution [36]; and/or
3) constrain the sparsity of $[g_i]$ [34], [37]–[39].

Kazemi *et al.* [40] used sparse BD to estimate source and receiver wavelets while processing seismic records acquired on land. The deconvolution algorithms in most of the geophysics literature handle somewhat impulsive source wavelets that are due to well-controlled sources, unlike the noisy and uncontrollable i.e., more realistic sources in this paper, about which we assume very little. It has to be observed that building initial estimate of $[g_i]$ is difficult for any algorithm, as the functional behaviors of $[d_i]$ and the actual $[g_i]$ are quite different from each other. Unlike standard methods, FBD does not require an extrinsic starting guess.

---

[2]Some seismic BD algorithms design deconvolution operators using an estimated subsurface velocity model [22], [23].

The Green's function retrieval is also the subject of *seismic interferometry* [41]–[46], where the cross-correlation (denoted by $\otimes$) between the records at two receivers with indices i and j,

$$d_{ij}(t) = \{d_i \otimes d_j\}(t) = \{s_a * g_{ij}\}(t), \qquad (2)$$

is treated as a proxy for the cross-correlated or *interferometric* Green's function $g_{ij} = g_i \otimes g_j$. Here $s_a = s \otimes s$ denotes the source auto-correlation. A classic result in interferometry states that a summation on the g_{ij} over various noisy sources, evenly distributed in space, will result in the Green's function due to a *virtual source* at one of the receivers [47]. In the absence of multiple evenly distributed noisy sources, the interferometric Green's functions can still be directly used for imaging [48]–[52], although this requires knowledge of the source signature. The above equation shows that the goal of interferometry, i.e., construction of g_{ij} given d_{ij}, is impeded by the source auto-correlation s_a. In an impractical situation with a zero-mean white noisy source, the d_{ij} would be precisely proportional to g_{ij}; but this is not at all realistic, so we don't assume a white source signature in FBD and eschew any concepts like virtual sources.

The failure of seismic noisy sources to be white[3] is already well known in seismic interferometry [45], [56]. To extract the response of a building, [57] proposes a deconvolution of the recorded waves at different locations in the building rather than the cross-correlation. Seismic interferometry by multi-dimensional deconvolution [58]–[61] uses an estimated interferometric point spread function as a deconvolution operator. The results obtained from this approach depend on the accuracy of the estimated point spread function, which relies on a uniform distribution of multiple noisy sources in space. In contrast to these seismic-interferometry-by-deconvolution approaches, FBD is designed to perform a *blind* deconvolution in the presence of a single noisy source and doesn't assume an even distribution of the noisy sources. In the presence of multiple noisy sources, as preprocessing to FBD, one has to use seismic blind source separation. For example, [62], [63] used independent component analysis for convolutive mixtures to decompose the multi-source recorded data into isolated records involving one source at a time.

The remainder of this paper is organized as follows. We explain the indeterminacy of unregularized BD problem in Section II. In Section III, we introduce FBD and argue that it can resolve this indeterminacy. This paper contains no theoretical guarantee, but we regard the formulation of such theorems as very interesting. In Section IV, we demonstrate the benefits of FBD using both idealized and practical synthetic seismic experiments.

II. MULTICHANNEL BLIND DECONVOLUTION

The z-domain representations are denoted in this paper using the corresponding capital letters. For example, the ith channel

output after a z-transform is denoted by

$$D_i(z) = \sum_{t=0}^{T} d_i(t) z^{-t}.$$

The traditional algorithmic approach to solve BD is a least-squares fitting of the channel output vector $[d_i : \{0, \ldots, T\} \to \mathbb{R}]$ to jointly optimize two functions i.e., the impulse response vector associated with different channels $[g_i : \{0, \ldots, \tau\} \to \mathbb{R}]$ and the source signature $s : \{0, \ldots, T - \tau\} \to \mathbb{R}$. The joint optimization can be suitably carried out using alternating minimization [64], [65]: in one cycle, we fix one function and optimize the other, and then fix the other and optimize the first. Several cycles are expected to be performed to reach convergence.

Definition 1 (LSBD: Least-squares Blind Deconvolution): It is a basic formulation that minimizes the least-squares functional:

$$U(s, [g_i]) = \sum_{k=1}^{n} \sum_{t=0}^{T} \{d_k(t) - \{s * g_k\}(t)\}^2; \qquad (3)$$

$$(\hat{s}, [\hat{g}_i]) = \arg\min_{s, [g_i]} U \qquad (4)$$

$$\text{subject to } \sum_{t=0}^{T} s^2(t) = 1. \qquad (5)$$

Here, $\hat{s}$ and $[\hat{g}_i]$ denote the predicted or estimated functions corresponding to the unknowns s and $[g_i]$, respectively. We have fixed the energy (i.e., sum-of-squares) norm of s in order to resolve the scaling ambiguity. In order to effectively solve this problem, it is required that the domain length $T + 1$ of the outputs d_i be much longer than the domain length $\tau + 1$ of the elements in the unknown vector $[g_i]$ [8].

Ill-posedness is the major challenge of BD, irrespective of the number of channels. For instance, when the number of channels $n = 1$, an undesirable minimizer for (3) would be the temporal Kronecker $\delta(t)$ for the impulse response, making the source signature equal the channel output. Even with $n \geq 1$, the LSBD problem can only be solved up to some indeterminacy. To quantify the ambiguity, consider that a filter $\phi(t) \neq \delta(t)$ and its inverse $\phi^{-1}(t)$ (where $\phi * \phi^{-1} = \delta$) can be applied to each element of $[g_i]$ and s respectively, and leave their convolution unchanged:

$$d_i(t) = \{s * g_i\}(t) = \{\{s * \phi^{-1}\} * \{g_i * \phi\}\}(t). \qquad (6)$$

If furthermore $s * \phi^{-1}$ and $[g_i * \phi]$ obey the constraints otherwise placed on s and $[g_i]$, namely in our case that s and each element of $[g_i]$ should have duration lengths $T - \tau + 1$ and $\tau + 1$ respectively, and the unity of the source energy, then we are in presence of a true ambiguity not resolved by those constraints. We then speak of ϕ as belonging to a set $\mathbb{Q}$ of undetermined filters. This formalizes the lack of uniqueness [8]: for any possibly desirable solution $(\hat{s}, [\hat{g}_i])$ and every $\phi \in \mathbb{Q}$, $(\hat{s} * \phi^{-1}, [\hat{g}_i * \phi])$ is an additional possibly undesirable solution. Taking all $\phi \in \mathbb{Q}$ spawns all solutions in a set $\mathbb{P}$ that equally minimize the least-squares functional in (3). Accordingly, in the z-domain, the elements in $[\hat{G}_i]$ of almost any solution in $\mathbb{P}$ share some common

---

[3]For example, the noise generated by drill bit operations is heavily correlated in time [53]–[55].

root(s), which are associated with its corresponding unknown filter $\Phi(z)$. In other words, the channel polynomials in $[\hat{G}_i]$ of nearly all the solutions are *not coprime*. A particular element in $\mathbb{P}$ has its corresponding $[\hat{G}_i]$ with the fewest common roots — we call it the *coprime* solution.

III. FOCUSED BLIND DECONVOLUTION

The aim of focused blind deconvolution is to seek the coprime solution of the LSBD problem. Otherwise, the channel polynomials of $[\hat{G}_i]$ will typically be *less sparse* and *less front-loaded* in the time domain owing to the common roots that are associated with the undetermined filter ϕ of (6). For example, including a common root r to the polynomials in $[\hat{G}_i]$ implies an additional factor $(z - r)$ that corresponds to subtracting $[r\, g_i(t)]$ from $[g_i(t + 1)]$ in the time domain, so that the sparsity is likely to reduce. Therefore, the intention and key innovation of FBD is to minimize the number of common roots in the channel polynomials of $[\hat{G}_i]$ associated with $\Phi(z)$. It is difficult to achieve the same result with standard ideas from sparse regularization. A simple justification of this is given in appendix A.

Towards this end, focused blind deconvolution solves a series of two least-squares optimization problems with focusing constraints. These constraints, described in the following subsections, can guide FBD to converge to the desired coprime solution. Note that this prescription does not guarantee that the recovered impulse responses should consistently match the true impulse responses;[4] nevertheless, we empirically encounter a satisfactory recovery in most practical situations of seismic inversion, as discussed below.

The first problem considers fitting the cross-correlated channel outputs to jointly optimize two functions i.e., the impulse-response cross-correlations between every possible channel pair and the source-signature auto-correlation. The focusing constraint in this problem will resolve the indeterminacy due to the amplitude spectrum of the unknown filter ϕ in (6) such that the impulse responses are *maximally white*. Then the second problem completes the focused blind deconvolution by fitting the above-mentioned impulse-response cross-correlations, to estimate $[g_i]$. The focusing constraint in this problem will resolve the indeterminacy due to the phase spectrum of the unknown filter ϕ such that $[g_i]$ is *maximally front-loaded*. As shown in the Fig. 1, these two problems will altogether resolve the indeterminacies of BD discussed in the previous section.

A. Focused Interferometric Blind Deconvolution

In order to isolate and resolve the indeterminacy due to the amplitude spectrum of $\phi(t)$, we consider a reformulated multi-channel blind deconvolution problem. This reformulation deals with the cross-correlated or interferometric channel outputs, $d_{ij} : \{-T, \ldots, T\} \to \mathbb{R}$, as in (2), between every possible channel pair (cf., [51]), therefore ending the indeterminacy due to the phase spectrum of $\phi(t)$.

Definition 2 (IBD: Interferometric Blind Deconvolution): We use this problem to lay the groundwork for the next problem, and

[4]In the seismic context, FBD does not guarantee that the recovered Green's function satisfies the wave equation with impulse source.

benchmarking. The optimization is carried out over the source-signature auto-correlation $s_a : \{-T + \tau, \ldots, T - \tau\} \to \mathbb{R}$ and the cross-correlated or interferometric impulse responses $g_{ij} : \{-\tau, \ldots, \tau\} \to \mathbb{R}$:

$$V(s_a, [g_{ij}]) = \sum_{k=1}^{n} \sum_{l=k}^{n} \sum_{t=-T}^{T} \{d_{kl}(t) - \{s_a * g_{kl}\}(t)\}^2; \quad (7)$$

$$(\hat{s}_a, [\hat{g}_{ij}]) = \arg\min_{s_a, [g_{ij}]} V$$

$$\text{subject to} \quad s_a(0) = 1; \quad s_a(t) = s_a(-t). \quad (8)$$

Here, we denoted the $(n + 1)n/2$-vector of unique interferometric impulse responses $[g_{11}, g_{12}, \ldots, g_{22}, g_{23}, \ldots, g_{nn}]$ by simply $[g_{ij}]$. We fit the interferometric outputs d_{ij} after max normalization while imposing $s_a(0) = 1$ to assist the convergence to a solution, where the necessary inequality condition $s_a(t) \le s_a(0)\, \forall\, t$ is satisfied. It also conveniently resolves the scaling ambiguity. More generally, the function $s_a(t)$ is the autocorrelation of $s(t)$ if and only if the Toeplitz matrix formed from its translates is positive semidefinite i.e., $\text{Toeplitz}(s_a) \succeq 0$. This is a result known as Bochner's theorem [66]. This semidefinite constraint could be realized by projecting $\text{Toeplitz}(s_a)$ onto the cone of positive semidefinite matrices at each iteration of the nonlinear least-squares iterative method [67]; however, in the numerical experiments, we observe convergence to acceptable solutions by just using the weaker constraints of IBD, when the data noise is sufficiently small. Moreover, employment of stronger constraints like $\text{Toeplitz}(s_a) \succeq 0$ increases the computational burden.

Similar to LSBD, IBD has unwanted minimizers obtained by applying a filter ψ^{-1} to s_a and ψ to each element of $[g_{ij}]$, but it is easily computed that ψ has to be *real and nonnegative* in the frequency domain ($|z| = 1$) and related to the amplitude spectrum of $\phi(t)$. Therefore, its indeterminacy is lesser compared to that of the LSBD approach.

Definition 3 (FIBD: Focused Interferometric Blind Deconvolution): FIBD starts by seeking a solution of the underdetermined IBD problem where the impulse responses are "maximally white", as measured by the concentration of their autocorrelation near zero lag (a Kronecker delta in lag defining pure whiteness). Towards that end, we use a regularizing term that penalizes the energy of the impulse-response auto-correlations proportional to the non-zero lag time t, before returning to solving the regular IBD problem.

$$W(s_a, [g_{ij}]) = V(s_a, [g_{ij}]) + \alpha \sum_{k=1}^{n} \sum_{t=-\tau}^{\tau} t^2 g_{kk}^2(t); \quad (9)$$

$$(\hat{s}_a, [\hat{g}_{ij}]) = \arg\min_{s_a, [g_{ij}]} W$$

$$\text{subject to} \quad s_a(0) = 1; \quad s_a(t) = s_a(-t). \quad (10)$$

Here, $\alpha \ge 0$ is an iteration-dependent regularization parameter. We consider a homotopy [68] approach to solve FIBD, where (10) is solved in succession for decreasing values of α, the result obtained for previous α being used as an initializer for the cycle that uses the current α. Note that a convergence to

---

Algorithm 1: Focused Interferometric Blind Deconvolution. Alternating Minimization of W, as in eq. 10, is Carried Out in Succession for Two Limits of α.

Preparation
  generate $[d_{ij}]$ and normalize with $d_{11}(0)$
Initialize
$$s_a(t) \leftarrow \begin{cases} 0, & \text{if } t \neq 0 \\ 1, & \text{otherwise} \end{cases}$$
$$g_{ij}(t) \leftarrow \begin{cases} 0, & \text{if } i = j \text{ and } t \neq 0 \\ \text{randn()}, & \text{if } i \neq j \text{ or } t = 0 \end{cases}$$
Strict Focusing (α going to ∞)
  $s_a, [g_{ij}] \leftarrow \underset{s_a,[g_{ij}]}{\arg\min}\, V(s_a, [g_{ij}])$
    s.t. $s_a(0) = 1$; $s_a(t) = s_a(-t)$;
       $\forall i g_{ii}(t) = 0$ whenever $t \neq 0$
Remove Focusing Constraint ($\alpha = 0$)
  $\hat{s}_a, [\hat{g}_{ij}] \leftarrow \underset{s_a,[g_{ij}]}{\arg\min}\, V(s_a, [g_{ij}])$
    s.t. $s_a(0) = 1$; $s_a(t) = s_a(-t)$;

---

the maximally-white solution is not guaranteed by merely decreasing α monotonically. Nonetheless, a convergence to acceptable impulse responses is observed in our numerical examples, where we start with extremely large values of α, before choosing $\alpha = 0$ and therefore ignoring the regularizing term. The effect of α going to ∞ is given by imposing strict focusing involving $g_{ii}(t) = 0$ whenever $t \neq 0$, while minimizing the V term. The entire workflow of FIBD is shown in Algorithm 1.

The focusing constraint resolves the indeterminacy of IBD. Minimizing the energy of the impulse-response autocorrelations g_{ii} proportional to the squared non-zero lag time will result in a solution where the impulse responses are heuristically as white as possible. In other words, FIBD minimizes the number of common roots, associated with the IBD indeterminacy $\Psi(z)$, in the estimated polynomials $\hat{G}_{ij}$, facilitating the goal of FBD to seek the coprime solution.

B. Focused Phase Retrieval

FIBD resolves a component of the LSBD ambiguity and estimates the interferometric impulse responses. This should be followed by phase retrieval (PR) — a least-squares fitting of $[\hat{g}_{ij}]$ to optimize $[g_i]$. The estimation of $[g_i]$ in PR is hindered by the unresolved LSBD ambiguity due to the phase spectrum of $\phi(t)$. In order to resolve the remaining ambiguity, we use a focusing constraint in PR.

Definition 4 (LSPR: Least-squares Phase Retrieval): Given the interferometric impulse response $[g_{ij}]$, the aim of the phase retrieval problem is to estimate unknown $[g_i]$.

$$X([g_i]) = \sum_{k=1}^{n} \sum_{l=i}^{n} \sum_{t=-\tau}^{\tau} \{\hat{g}_{kl}(t) - \{g_k \otimes g_l\}(t)\}^2; \quad (11)$$

$$[\hat{g}_i] = \underset{[g_i]}{\arg\min}\quad X \quad (12)$$

Algorithm 2: Focused Phase Retrieval. Solving Y in eq. 14 With Strict Focusing, Then Solving X in eq. 11.

Preparation
  get $[\hat{g}_{ij}]$ using FIBD in Algorithm 1
Parameters
Initialize
$$g_i(t) \leftarrow \begin{cases} 0, & \text{if } i = f \text{ and } t \neq 0 \\ \text{randn()}, & \text{if } i \neq f \text{ or } t = 0 \end{cases}$$
Strict Focusing (β going to ∞)
  $[g_i] \leftarrow \underset{[g_i]}{\arg\min}\, Y([g_i])$
    s.t. $g_f(t) = 0$ whenever $t \neq 0$ **Remove**
Focusing Constraint ($\beta = 0$)
  $[\hat{g}_i] \leftarrow \underset{[g_i]}{\arg\min}\, X([g_i])$

LSPR is ill-posed. Consider a *white* filter $\chi(t) \neq \delta(t)$, where $\chi \otimes \chi = \delta$, that can be applied to each of the impulse responses, and leave their cross-correlations unchanged:

$$g_{ij}(t) = \{g_i \otimes g_j\}(t) = \{\{g_i * \chi\} \otimes \{g_j * \chi\}\}(t). \quad (13)$$

If furthermore $g_i * \chi$ obeys the constraint otherwise placed, namely in our case that the impulse responses should have duration length τ, then we are in the presence of a true ambiguity not resolved by this constraint. It is obvious that the filter $\chi(t)$ is linked to the remaining unresolved component of the LSBD indeterminacy, i.e., the phase spectrum of $\phi(t)$.

Definition 5 (FPR: Focused Phase Retrieval): FPR seeks a solution of the under-determined LSPR problem where $[g_i]$ is "maximally front-loaded". It starts with an optimization that fits the interferometric impulse responses only linked with the most front-loaded channel[5] f, before returning to solving the regular LSPR problem. We use a regularizing term that penalizes the energy of the most front-loaded response g_f proportional to the time $t \neq 0$:

$$Y([g_i]) = \sum_{k=1}^{n} \sum_{t=-\tau}^{\tau} \{\hat{g}_{kf}(t) - \{g_k \otimes g_f\}(t)\}^2$$

$$+ \beta \sum_{t=0}^{\tau} g_f^2(t)t^2; \quad (14)$$

$$[\hat{g}_i] = \underset{g_i}{\arg\min}\quad Y. \quad (15)$$

Here, $\beta \geq 0$ is an iteration-dependent regularization parameter. Again, we consider a homotopy approach to solve this optimization problem. We start with extremely large values of β, before choosing $\beta = 0$ and therefore ignoring the regularizing term. The effect of β going to ∞ is given by imposing strict focusing involving $g_f(t) = 0$ whenever $t \neq 0$. while minimizing the Y term. The entire workflow of FPR is shown in Algorithm 2.

FPR chooses the undetermined filter χ such that $g_i * \chi$ has the energy maximally concentrated or focused at the front (small

---

[5]In the seismic context, the most front-loaded channel corresponds to the closest receiver $i = f$ to the noisy source, assuming that the traveltime of the waves propagating from the source to this receiver is the shortest.

TABLE I
TIME COMPLEXITY OF A SINGLE ITERATION. HERE, M DENOTES THE LENGTH
OF THE ZERO-PADDED SIGNALS AND n DENOTES THE NUMBER OF CHANNELS

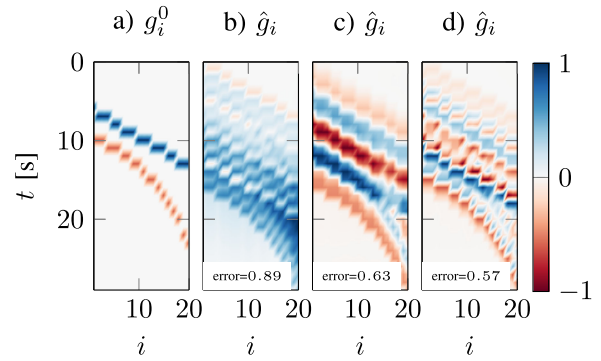| Algorithm	Complexity
LSBD	$\mathcal{O}(n\,M\log M)$
FIBD/IBD	$\mathcal{O}(n^2\,M\log M)$
FPR/PR	$\mathcal{O}(n^2\,M\log M)$

Fig. 2. Idealized Experiment I. The results are displayed as images that use the full range of colors in a colormap. Each pixel of these images corresponds to a time t and a channel index i. Impulse responses a) true; b)—d) undesired.

t). Minimizing the second moment of the squared impulse responses will result in a solution where the impulse responses are as front-loaded as possible. Counting on the estimated impulse responses from FPR, we return to the LSBD formulation in order to finalize the BD problem.

C. Sufficiently Dissimilar Channel Configuration

FBD seeks the coprime solution of the ill-posed LSBD problem. Therefore, for the success of FBD, it is important that the true transfer functions do not share any common zeros in the z-domain. This requirement is satisfied when the channels are chosen to be *sufficiently dissimilar*. The channels are said to be sufficiently dissimilar unless there exist a spurious γ and $[g_i]$ such that the true impulse-response vector $[g_i^0] = [\gamma * g_i]$. Here, γ is a filter that

1) is independent of the channel index i;
2) belongs to the set $\mathbb{Q}$ of filters that cause indeterminacy of the LSBD problem;
3) doesn't simply shift g_i in time.

In our experiments, FBD reconstructs a good approximation of the true impulse responses if the channels are sufficiently dissimilar. Otherwise, FBD outputs an undesirable solution ($s^0 * \gamma^{-1}, [g_i]$), as opposed to the desired ($s^0, [\gamma * g_i]$), where s^0 is the true source signature. In the next section, we will show numerical examples with both similar and dissimilar channels.

IV. NUMERICAL SIMULATIONS

We have made a documented source code available, for reproducibility of these simulations, through a Julia [69] package FocusedBlindDecon [70]. This software uses the fast Fourier transform on the zero-padded signals in order to perform convolutions and cross-correlations, resulting in the time complexities of Table I. In this code, the linear systems encountered during the alternating minimization of LSBD, IBD and FIBD are solved using the LSMR algorithm [71], provided by the IterativeSolvers package, while the optimizations in LSPR and FPR are carried out using a conjugate gradient algorithm in the Optim [72] package.

A. Idealized Experiment I

We consider an experiment with $n = 20$, $\tau = 30$ and $T = 600$. The aim is to reconstruct the true impulse-response vector $[g_i^0]$, plotted in Fig. 2a, from the channel outputs generated using a Gaussian random source signature s^0. The impulse responses of similar kind are of particular interest e.g., in seismic inversion and room acoustics as they reveal the arrival of energy, propagated from an impulsive source, at the receivers in the medium.

In this case, the arrivals have onsets of 6 s and 10 s at the first channel and they curve linearly and hyperbolically, respectively. The linear arrival is the earliest arrival that doesn't undergo scattering. The hyperbolic arrival is likely to represent a wave that is reflected or scattered from an interface between two materials with different acoustic impedances.

LSBD: To illustrate its non-uniqueness, we use three different initial estimates of s and $[g_i]$ to observe convergence to three different solutions that belong to $\mathbb{P}$ (Section II). During the first alternating minimization, the channel-output misfit (given in (3)), which is plotted as a function of the iteration count in Fig. 3a, decreases approximately linearly. Similarly, the misfit in the impulse responses (after neglecting an overall translation in time) is plotted in Fig. 3b. At the convergence, the channel-output misfit in all the three cases $U(\hat{s}, [\hat{g}_i]) \lesssim 10^{-5}$, whereas the impulse-response misfit is greater than 0.5, justifying non-uniqueness. The channel responses corresponding to the three solutions are plotted in Figs. 2b–d, where we notice that none of the solutions is desirable due to insufficient resolution.

FIBD: In order to isolate the indeterminacy due to the amplitude spectrum of the unknown filter $\phi(t)$ in (6) and justify the use of the focusing constraint in (9), we plot the true and undesirable impulse responses after cross-correlation in the Fig. 4. It can be easily noticed that the true impulse-response autocorrelation $g_1^0 \otimes g_1^0$ is more focused at $t = 0$ than the undesirable impulse-response autocorrelations $\hat{g}_1 \otimes \hat{g}_1$. The defocusing is caused by the ambiguity related to the amplitude spectrum of $\phi(t)$. FIBD in Algorithm 1 with $\vec{\alpha} = [\infty, 0]$ resolves this ambiguity and satisfactorily recovers the true interferometric impulse-response vector $[g_{ij}^0]$, as plotted in Fig. 5a. The convergence plots of this algorithm in Figs. 3c and 3d show that the final misfit in $[d_{ij}]$ is approximately less than 10^{-7} and the final misfit in $[g_{ij}]$ is less than 10^{-1}. We recognize the FIBD recovery to be satisfactory in Fig. 5b regardless of the Gaussian white noise that is added to the channel outputs at signal-to-noise (SNR) 1 dB. For quantitative comparison, our plots also show the relative least-squares error between the true and estimated responses.

FPR: In order to motivate the use of the second focusing constraint, we plotted the normalized cumulative energy of the true and undesired impulse responses in Fig. 6. It can be
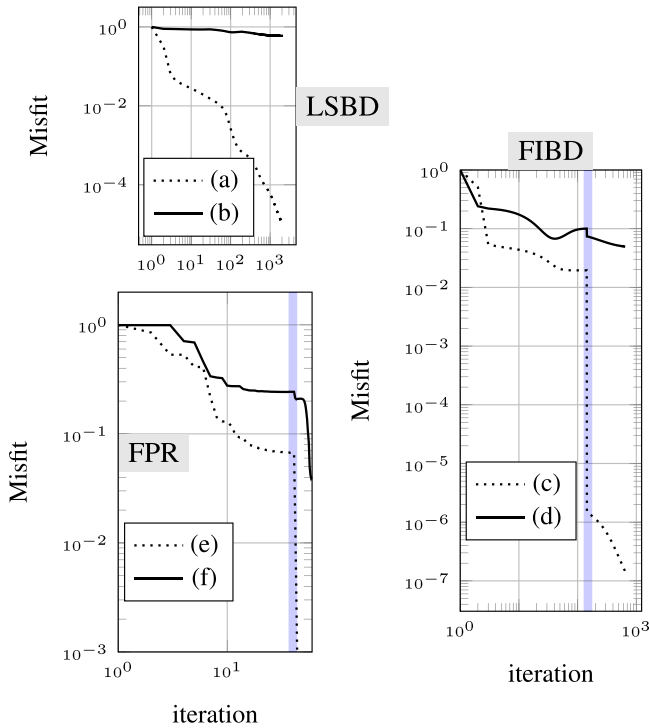
Fig. 3. Least-squares misfits are plotted as a function of the iteration count for the Idealized Experiment I. LSBD: a) misfit in $[d_i]$, given by U; b) misfit in $[g_i]$. FIBD: c) misfit in $[d_{ij}]$, given by V; d) misfit in $[g_{ij}]$. FPR: e) misfit in $[g_{ij}]$, given by X; f) misfit in $[g_i]$, after neglecting an overall translation in time. In the case of FIBD and FPR, the blue vertical line represents the transition of the regularization parameter from ∞ to 0.
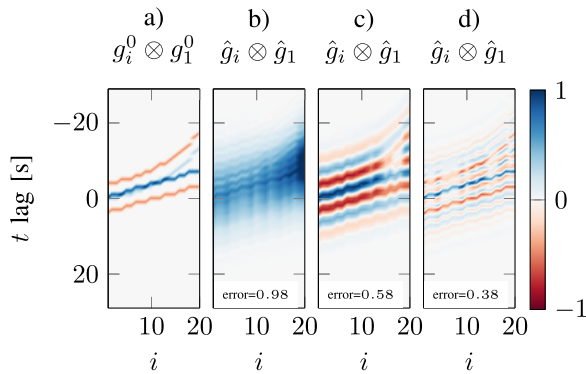

Fig. 4. Idealized Experiment I. Cross-correlations of impulse responses corresponding to the Fig. 2: a) true; b)—d) undesired.

easily noticed that the fastest rate of energy buildup in time occurs in the case of the true impulse responses. In other words, the energy of the true impulse responses is more front-loaded compared to undesired impulse responses. The FPR in Algorithm 2 with $\vec{\beta} = [\infty, 0]$ satisfactorily recovers $[g_i^0]$ that is plotted in: the Fig. 5c — utilizing $[g_{ij}]$ recovered from the noiseless channel outputs (Fig. 5a); the Fig. 5d — utilizing $[g_{ij}]$ recovered from the channel outputs (Fig. 5b) with Gaussian white noise. The convergence of this algorithm is shown in the Figs. 3 e and 3f. Note that the overall time translation and scaling cannot be fundamentally determined.
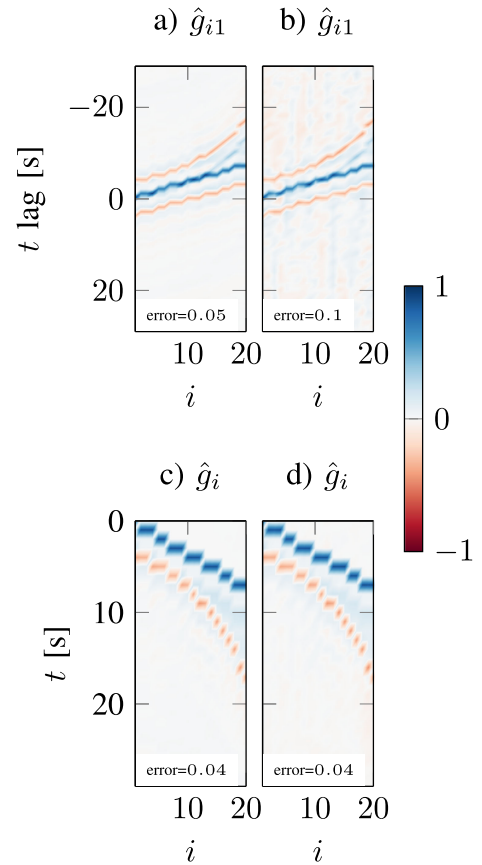

Fig. 5. Idealized Experiment I. a) FIBD estimated interferometric impulse responses corresponding to Fig. 4a, after fitting the interferometric channel outputs. b) Same as (a), except after white noise is added to the channel outputs. c) Estimated impulse responses from FPR by fitting the FIBD-outcome interferometric impulse responses in (a). d) Same as (c), except fitting the FIBD outcome in (b).
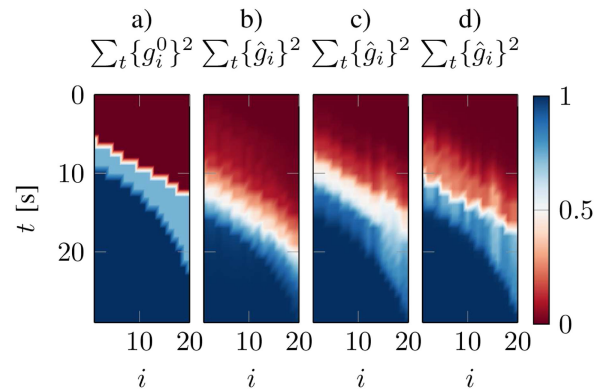

Fig. 6. Idealized Experiment I. Normalized cumulative energy of: a) true; b)—d) undesired impulse responses corresponding to Fig. 2.

B. Idealized Experiment II

This IBD-benchmark experiment with $n = 20$ $\tau = 30$ and $T = 600$ aims to reconstruct simpler interferometric impulse responses, plotted in Fig. 7b, corresponding to the true impulse responses in Fig. 7a. A satisfactory recovery of $[g_{ij}^0]$ wasn't

a) g_i^0

b) g_{i1}^0 **c)** $\hat{g}_{i1}$ **d)** $\hat{g}_{i1}$
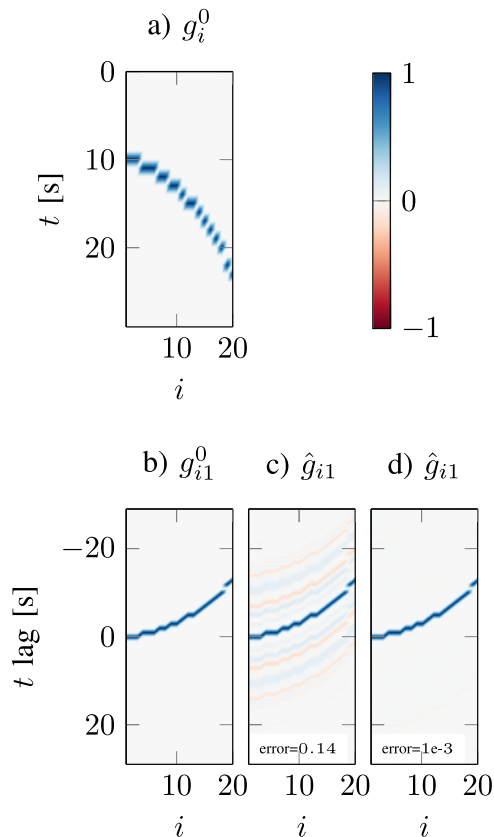
Fig. 7. Idealized Experiment II. a) True impulse responses. Interferometric impulse responses: b) true; c) estimated using IBD; d) estimated using FIBD.

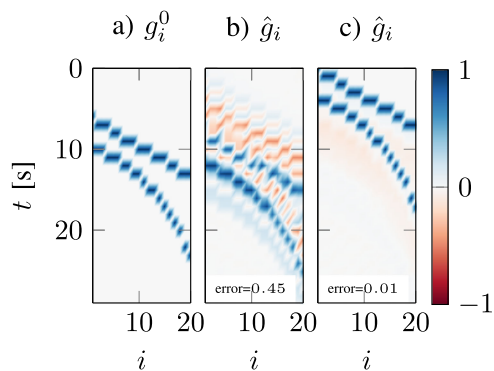**a)** g_i^0 **b)** $\hat{g}_i$ **c)** $\hat{g}_i$

Fig. 8. Idealized Experiment III. a) True impulse responses. b) Estimated impulse responses using LSPR. c) Estimated impulse responses using FPR.

achievable without the focusing constraint — the IBD outcome (higher error) in the Fig. 7c doesn't match the true interferometric impulse responses in the Fig. 7b, unlike FIBD (lower error) in the Fig. 7d.

C. Idealized Experiment III

We consider another experiment with $n = 20$ and $\tau = 30$ to reconstruct the true impulse-response vector $[g_i^0]$ (plotted in Fig. 8a) by fitting their cross-correlations in $[g_{ij}^0]$. A satisfactory recovery of $[g_i^0]$ from $[g_{ij}^0]$ wasn't achievable without the

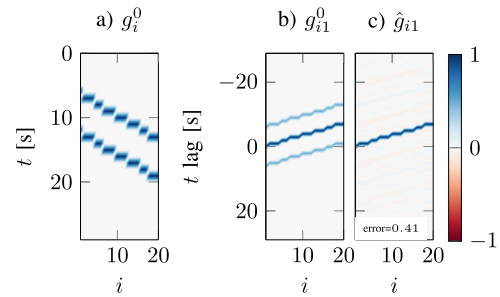**a)** g_i^0 **b)** g_{i1}^0 **c)** $\hat{g}_{i1}$

Fig. 9. Idealized Experiment IV. a) True impulse responses of channels that are not sufficiently dissimilar. b) True interferometric impulse responses corresponding to (a). c) FIBD estimated interferometric impulse responses corresponding to (b), after fitting the interferometric channel outputs.

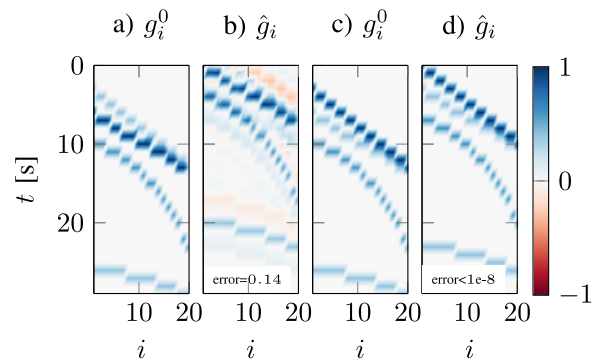**a)** g_i^0 **b)** $\hat{g}_i$ **c)** g_i^0 **d)** $\hat{g}_i$

Fig. 10. Idealized Experiment V. a) True impulse responses that are not front-loaded. b) FPR estimated impulse responses corresponding to (a), after fitting the true interferometric impulse responses. c) Same as (a), but front-loaded. d) Same as (b), but corresponding to (c). The estimated relative least-squares error neglects an overall translation in time.

focusing constraint — the outcome of LSPR (higher error), in Fig. 8b, doesn't match the true impulse responses, in Fig. 8a, but is contaminated by the filter $\chi(t)$ in (13). On the other hand, FPR results (lower error) in the outcome (Fig. 8c) that is not contaminated by $\chi(t)$.

D. Idealized Experiment IV

This experiment with $n = 20$, $\tau = 30$ and $T = 600$ aims to reconstruct the true interferometric impulse responses, plotted in Fig. 9b, corresponding to the true impulse responses in Fig. 9a. The outcome of FIBD with $\vec{\alpha} = [\infty, 0]$, plotted in Fig. 9c, has high error and doesn't clearly match the true interferometric impulse responses because the channels are *not* sufficiently dissimilar. In this regard, observe that Fig. 9a true impulse responses at various channels i differ only by a fixed time-translation instead of curving as in Fig. 2a.

E. Idealized Experiment V

We consider another experiment with $n = 20$ and $\tau = 30$ to reconstruct the true impulse-response vector $[g_i^0]$ (plotted in Fig. 10a) that are *not* front-loaded, by fitting their cross-correlations in $[g_{ij}^0]$. The FPR estimated impulse-response vector $[\hat{g}_i]$, plotted in Fig. 10b, has high error and doesn't clearly depict
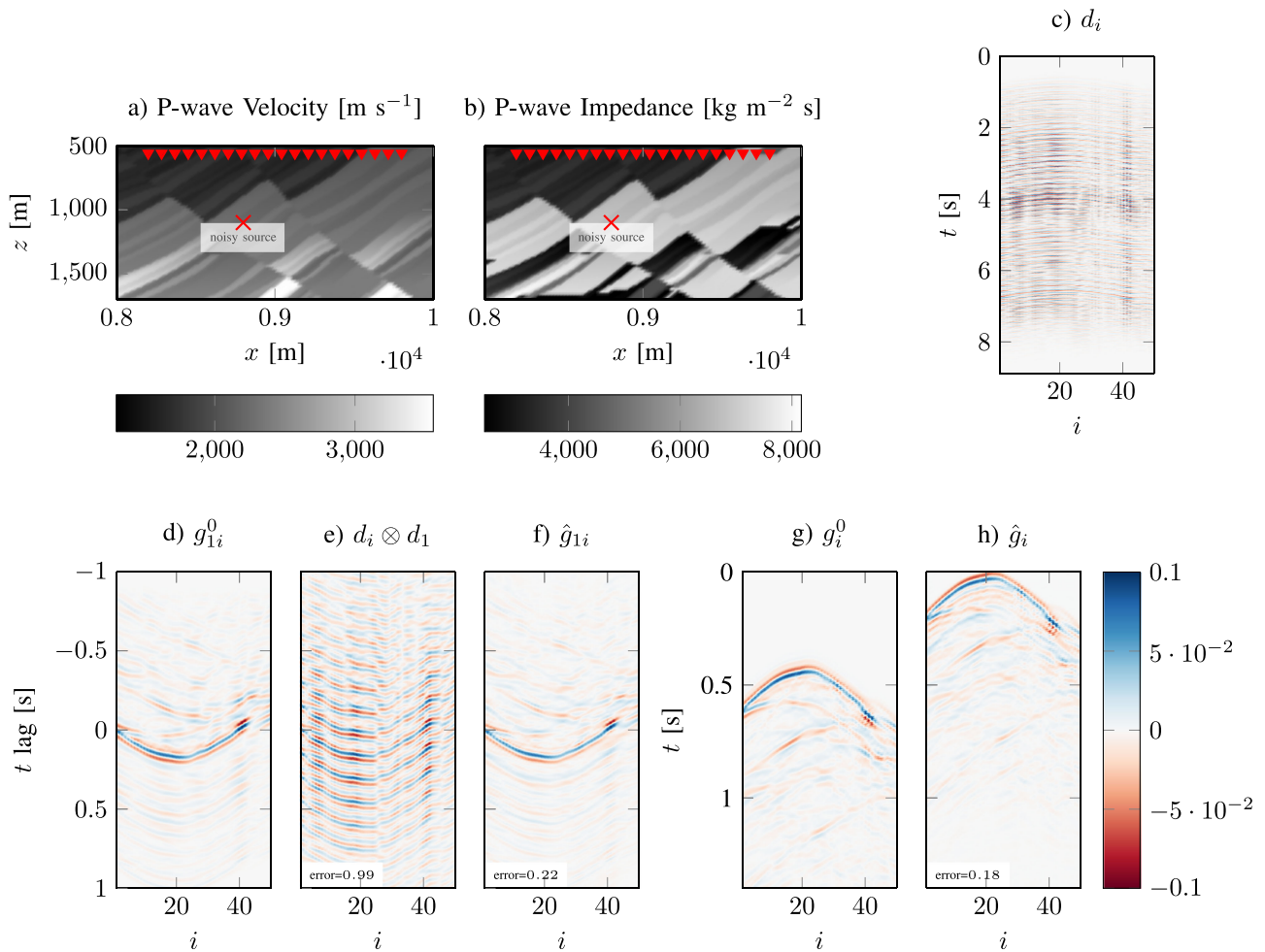
Fig. 11. Marmousi Seismic Experiment. a) Acoustic velocity model for wave propagation. b) Acoustic impedance model depicting interfaces that reflect waves. c) Recorded seismic data at 50 receivers. d) True interferometric Green's functions. e) Seismic interferometry by cross-correlation. f) FIBD estimated interferometric Green's functions. g) True Green's functions. h) FBD estimated Green's functions. The estimated relative least-squares error neglects an overall translation in time.

the arrivals because there exists a spurious $\chi \neq \delta$ obeying (13), such that $[g_i^0 * \chi]$ is more front-loaded than $[g_i^0]$. We observe that FPR typically doesn't result in a favorable outcome if the impulse responses are not front-loaded. Otherwise, the front-loaded $[g_i^0]$, plotted in Fig. 10c, is successfully reconstructed in Fig. 10d, except for an overall translation in time.

V. GREEN'S FUNCTION RETRIEVAL

Finally, we consider a more realistic scenario involving seismic-wave propagation in a complex 2-D structural model, which is known as the Marmousi model [73] in exploration seismology. The Marmousi P-wave velocity and impedance plots are in Figs. 11a and 11b, respectively. We inject an unknown band-limited source signal, e.g., due to a drill bit, into this model for 8.8 s, such that $T = 1121$. The signal's auto-correlation and power spectrum are plotted in Figs. 12a and 12b, respectively. Note that the source signal is correlated and the model used to generate this signal is given in the Appendix B. We used an acoustic time-domain staggered-grid finite-difference solver
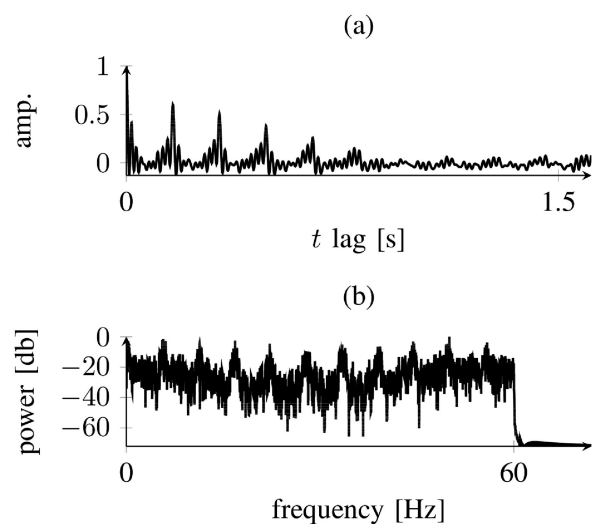

Fig. 12. Source signature for the seismic experiment.(a) auto-correlation that contaminates the interferometric Green's functions in the time domain — only 16% of T is plotted; (b) power spectrum, where the Nyquist frequency is 60 Hz.

for wave-equation modeling. The recorded seismic data at fifty receivers spaced 32.65 m apart, placed at a depth of 560 m, can be modeled as the output of a linear system that convolves the source signature with the Earth's impulse response, i.e., its Green's function. As plotted in the Fig. 11c, the modeled seismic data are hard to interpret. We recall that in the seismic context:

1) the impulse responses in $[g_i]$ correspond to the unique subsurface Green's function $g(\vec{x}, t)$ evaluated at the receiver locations in $[\vec{x}_i]$, where the seismic-source signals are recorded;

2) the channel-output vector $[d_i]$ corresponds to the noisy subsurface wavefield $d(\vec{x}, t)$ recorded at the receivers only for $\{0, \ldots, T\}$ — we are assuming that the source may be arbitrarily on or off throughout this time interval, just as in usual drilling operations;

3) τ denotes the propagation time necessary for the seismic energy, including multiple scattering, traveling from the source to a total of n receivers, to decrease below an ad-hoc threshold.

The goal of this experiment is to reconstruct the subsurface Green's function vector $[g_i]$ that contains:

1) the direct arrival from the source to the receivers and

2) the reflected waves from various interfaces in the model.

We casually chose the propagation time to be 1.5 s ($\tau = 187$), after observing that the subsequent scattered energy was sufficiently low; our results were not sensitive to this parameter.

The 'true' Green's functions g_i^0 and the interferometric Green's functions g_{ij}^0, in Figs. 11g and 11d, are generated following these steps:

1) get data for 1.5 s using a Ricker source wavelet (basically a degree-2 Hermite function modulated to a peak frequency of 20 Hz);

2) create cross-correlated data necessary for $[g_{ij}^0]$; and

3) perform a deterministic deconvolution on the data using the Ricker wavelet.

Seismic interferometry by cross-correlation (see (2)) fails to retrieve direct and the scattered arrivals in the true interferometric Green's functions, as the cross-correlated data $[d_{ij}]$, plotted in Fig. 11 e, is contaminated by the auto-correlation of the source signature (Fig. 12a) and therefore high error. Therefore, we use FBD to first extract the interferometric Green's functions by FIBD, plotted in the Fig. 11f, and then recover the Green's functions, plotted in the Fig. 11h, using FPR. Notice that the FBD estimated Green's functions have lower error and clearly depict the direct and the scattered arrivals, confirming that our method doesn't suffer from the complexities in the subsurface models.

VI. CONCLUSION

Focused blind deconvolution (FBD) solves a series of two optimization problems in order to perform multichannel blind deconvolution (BD), where both the unknown impulse responses and the unknown source signature are estimated given the channel outputs. It is designed for a BD problem where the impulse responses are supposed to be sparse, front-loaded and shorter in duration compared to the channel outputs; as in the case of

seismic inversion with a noisy source. The optimization problems use focusing constraints to resolve the indeterminacy inherent to the traditional BD. The first problem considers fitting the interferometric channel outputs and focuses the energy of the impulse-response auto-correlations at the zero lag to estimate the interferometric impulse responses and the source auto-correlation. The second problem completes FBD by fitting the estimated interferometric impulse responses, while focusing the energy of the most front-loaded channel at the zero time. FBD doesn't require any support constraints on the unknowns. We have demonstrated the benefits of FBD using seismic experiments and made the source code available for reproducibility.

APPENDIX A
FOCUSING VS ℓ_1

In this appendix, we present a simple justification of the ability of the focusing functional (9) on the autocorrelation to select for sparsity, in a setting where ℓ_1 minimization is unable to do so. We consider the special case of a sparse impulse-response vector with *nonnegative* entries, made less sparse after convolution with an undetermined vector of (6) that has nonnegative entries as well. This scenario is not fully representative of the more general formulation assumed in this paper, where cancellations may occur because of alternating signs. It seems necessary, however, to make an assumption of no cancellation (like positivity) in order to obtain the type of comparison result that we show in this section.

Consider two infinite sequences g_i^0 and ϕ_j, for $i, j \in \mathbb{Z}$ (the set of integers), with sufficient decay so that all the expressions below make sense, and all the sum swaps are valid. Assume that $g_i^0 \geq 0$ and $\phi_i \geq 0$ for all $i \in \mathbb{Z}$, not identically zero. Let

$$g_j = (g^0 * \phi)_j = \sum_{i \in \mathbb{Z}} g_i^0 \phi_{j-i},$$

which obviously also obeys $g_i \geq 0$ for all $i \in Z$. Assume the normalization condition $\sum_{i \in \mathbb{Z}} \phi_i = 1$.

Now consider the autocorrelations

$$G_j^0 = (g^0 \otimes g^0)_j = \sum_i g_i^0 g_{j+i}^0,$$

$$G_j = (g \otimes g)_j = \sum_i g_i g_{j+i},$$

and a specific choice of focusing functional,

$$F^0 = \sum_{j \in Z} j^2 G_j^0, \quad F = \sum_{j \in \mathbb{Z}} j^2 G_j.$$

Proposition 1:

$$F \geq F^0,$$

with equality if and only if ϕ_i is the Kronecker δ_{i0}.

Proof: All sums run over $\mathbb{Z}$. Start by observing

$$F^0 = \sum_j \sum_k K_{jk} g_j^0 g_k^0, \quad K_{jk} = (j-k)^2,$$

and

$$F = \sum_j \sum_k L_{jk} g_j^0 g_k^0,$$

$$L_{jk} = \sum_m \sum_n ((j-k)-(m-n))^2 \, \phi_m \phi_n.$$

For any particular value $m - n = a$, we have

$$\sum_j \sum_k ((j-k)-a)^2 \, g_j^0 g_k^0$$

$$= a^2 \sum_j \sum_k g_j^0 g_k^0 + \sum_j \sum_k (j-k)^2 g_j^0 g_k^0$$

$$\geq F^0,$$

(the term linear in $j - k$ drops because $j - k$ is antisymmetric in j and k, while $g_j^0 g_k^0$ is symmetric), with equality if and only if $a = 0$.

Now F is a convex combination of such contributions:

$$\sum_m \sum_n \left[\sum_j \sum_k ((j-k)-(m-n))^2 \, g_j^0 g_k^0 \right] \phi_m \phi_n$$

$$\geq \sum_m \sum_n \left[F^0 \right] \phi_m \phi_n$$

$$= F^0$$

with equality if and only if the cartesian product supp $\phi \times$ supp ϕ contains only the diagonal $m = n$. This latter scenario only arises when supp $\phi = \{0\}$, which is only compatible with $\sum_i \phi_i = 1$ when $\phi_i = \delta_{i0}$. ∎

In contrast, notice that $\sum_i g_i^0 = \sum_i g_i$, hence g^0 and g cannot be discriminated with the ℓ_1 norm. The ℓ_1 norm is unable to measure the extent to which the support of g^0 was "spread" by convolution with ϕ, when $\sum \phi_i = 1$, and when all the functions are nonnegative.

The continuous counterpart of this result, for nonnegative functions $g^0(t)$ and $g(t) = \int g^0(s)\phi(t-s)ds$, with nonnegative ϕ such that $\int \phi(t)dt = 1$ in the sense of measures, involves the autocorrelations

$$G^0(t) = (g^0 \otimes g^0)(t) = \int g^0(s)g^0(s+t)ds,$$

$$G(t) = (g \otimes g)(t),$$

and focusing functionals

$$F^0 = \int t^2 G^0(t)dt, \qquad F = \int t^2 G(t)dt.$$

Then, $F \geq F^0$, with equality if and only if $\phi(t) = \delta(t)$, the Dirac delta.

APPENDIX B
DRILL-BIT SOURCE SIGNATURE

We now clarify the model used to generate a correlated random drill-bit signal for the numerical experiment of Section V. First, a band-limited random signal $r(t)$ of length T

is generated using random i.i.d. variables $X_k \sim N(0, \sigma^2)$ and $Y_k \sim P(-\pi, \pi)$ in the frequency ω domain as:

$$R(\omega) = \sum_k X_k \, \exp(\imath Y_k) \, \mathrm{sinc}(\omega T - 2\pi k).$$

Here, N denotes a Gaussian distribution with zero mean and standard deviation σ, and P denotes a uniform distribution such that $|Y_k| \leq \pi$. Then, in order to induce correlation, we added several arbitrarily time-translated copies of $r(t)$ together. Finally, the drill-bit source signal $s(t)$ is given by applying a suitable tapered time window to the sum.

REFERENCES

[1] F. Aminzadeh and S. N. Dasgupta, *Geophysics for Petroleum Engineers*, vol. 60. Amsterdam, The Netherlands: Elsevier, 2013.

[2] J. Liu and H. Malvar, "Blind deconvolution of reverberated speech signals via regularization," in *Proc. IEEE Int. Conf. Acoust., Speech, Signal Process.*, 2001, vol. 5, pp. 3037–3040.

[3] T. Yoshioka *et al.*, "Making machines understand us in reverberant rooms: Robustness against reverberation for automatic speech recognition," *IEEE Signal Process. Mag.*, vol. 29, no. 6, pp. 114–126, Nov. 2012.

[4] S Amari, S. C. Douglas, A. Cichocki, and H. H. Yang, "Multichannel blind deconvolution and equalization using the natural gradient," in *Proc. 1st IEEE Signal Process. Workshop Signal Process. Adv. Wireless Commun.*, 1997, pp. 101–104.

[5] S. C. Douglas, A. Cichocki, and S.-I. Amari, "Multichannel blind separation and deconvolution of sources with arbitrary distributions," in *Proc. IEEE Workshop Neural Netw. Signal Process.*, 1997, pp. 436–445.

[6] F. Sroubek and J. Flusser, "Multichannel blind iterative image restoration," *IEEE Trans. Image Process.*, vol. 12, no. 9, pp. 1094–1106, Sep. 2003.

[7] P. Bharadwaj, L. Demanet, and A. Fournier, "Focused blind deconvolution of interferometric Green's functions, " in, *SEG Tech. Program Expanded Abstracts*. Tulsa, OK, USA: Society of Exploration Geophysicists, 2018.

[8] G. Xu, H. Liu, L. Tong, and T. Kailath, "A least-squares approach to blind channel identification," *IEEE Trans. Signal Process.*, vol. 43, no. 12, pp. 2982–2993, Dec. 1995.

[9] S. Subramaniam, A. P. Petropulu, and C. Wendt, "Cepstrum-based deconvolution for speech dereverberation," *IEEE Trans. Speech Audio Process.*, vol. 4, no. 5, pp. 392–396, Sep. 1996.

[10] Y. A. Huang and J. Benesty, "Adaptive multi-channel least mean square and newton algorithms for blind channel identification," *Signal Process.*, vol. 82, no. 8, pp. 1127–1138, 2002.

[11] N. D. Gaubitch, J. Benesty, and P. A. Naylor, "Adaptive common root estimation and the common zeros problem in blind channel identification," in *Proc. 13th Eur. Signal Process. Conf.*, 2005, pp. 1–4.

[12] A. W. Khong, X. Lin, and P. A. Naylor, "Algorithms for identifying clusters of near-common zeros in multichannel blind system identification and equalization," in *Proc. IEEE Int. Conf. Acoust., Speech Signal Process.*, 2008, pp. 389–392.

[13] D. Kundur and D. Hatzinakos, "Blind image deconvolution," *IEEE Signal Process. Mag.*, vol. 13, no. 3, pp. 43–64, May 1996.

[14] P. Campisi and K. Egiazarian, *Blind Image Deconvolution: Theory and Applications*. Boca Raton, FL, USA: CRC Press, 2016.

[15] A. Ahmed, A. Cosse, and L. Demanet, "A convex approach to blind deconvolution with diverse inputs," in *Proc. IEEE 6th Int. Workshop Comput. Adv. Multi Sensor Adaptive Process.*, 2015, pp. 5–8.

[16] X. Li, S. Ling, T. Strohmer, and K. Wei, "Rapid, robust, and reliable blind deconvolution via nonconvex optimization," *Appl. Computational Harmon. Anal.*, 2018.

[17] A. Ahmed and L. Demanet, "Leveraging diversity and sparsity in blind deconvolution," *IEEE Trans. Inf. Theory*, vol. 64, no. 6, pp. 3975–4000, 2018.

[18] J. Romberg, N. Tian, and K. Sabra, "Multichannel blind deconvolution using low rank recovery," *Proc. SPIE*, vol. 8750, 2013, Art. no. 87500E.

[19] L. Tong, G. Xu, and T. Kailath, "Blind identification and equalization based on second-order statistics: A time domain approach," *IEEE Trans. Inf. Theory*, vol. 40, no. 2, pp. 340–349, Mar. 1994.

[20] L. Tong, G. Xu, B. Hassibi, and T. Kailath, "Blind channel identification based on second-order statistics: A frequency-domain approach," *IEEE Trans. Inf. Theory*, vol. 41, no. 1, pp. 329–334, Jan. 1995.

[21] L. Tong and S. Perreau, "Multichannel blind identification: From subspace to maximum likelihood methods," *Proc. IEEE*, vol. 86, no. 10, pp. 1951–1968, Oct. 1998.

[22] D. Miller and J. Haldorsen, "Methods for deconvolution of unknown source signatures from unknown waveform data," U.S. Patent 4 922 362, 1990.

[23] J. B. Haldorsen, D. E. Miller, and J. J. Walsh, "Walk-away VSP using drill noise as a source," *Geophysics*, vol. 60, no. 4, pp. 978–997, 1995.

[24] Y. Zhang, Y. Lau, H.-W. Kuo, S. Cheung, A. Pasupathy, and J. Wright, "On the global geometry of sphere-constrained sparse blind deconvolution," in *Proc. IEEE Conf. Comput. Vis. Pattern Recognit.*, 2017, pp. 4894–4902.

[25] Y. Li and Y. Bresler, "Global geometry of multichannel sparse blind deconvolution on the sphere," in *Proc. Adv. Neural Inf. Process. Syst.*, 2018, pp. 1132–1143.

[26] T. J. Ulrych, D. R. Velis, and M. D. Sacchi, "Wavelet estimation revisited," *Leading Edge*, vol. 14, no. 11, pp. 1139–1143, 1995.

[27] X. Liu and H. Liu, "Survey on seismic blind deconvolution," *Progress Geophys.*, vol. 18, no. 2, pp. 203–209, 2003.

[28] M. Van der Baan and D.-T. Pham, "Robust wavelet estimation and blind deconvolution of noisy surface seismics," *Geophysics*, vol. 73, pp. V37–V46, 2008.

[29] E. A. Robinson, "Predictive decomposition of seismic traces," *Geophysics*, vol. 22, no. 4, pp. 767–778, 1957.

[30] H. Wold, "A study in the analysis of stationary time series," Ph.D. dissertation, Almqvist & Wiksell, Stockholm, Sweden, 1938.

[31] E. A. Robinson and S. Treitel, *Geophysical Signal Analysis*. Englewood Cliffs, NJ, USA: Prentice-Hall, 1980, vol. 263.

[32] Ö. Yilmaz, *Seismic Data Analysis*, vol. 1. Tulsa, OK, USA: Soc. of Exploration Geophysicists, 2001.

[33] K. F. Kaaresen and T. Taxt, "Multichannel blind deconvolution of seismic signals," *Geophysics*, vol. 63, no. 6, pp. 2093–2107, 1998.

[34] N. Kazemi and M. D. Sacchi, "Sparse multichannel blind deconvolution," *Geophysics*, vol. 79, no. 5, pp. V143–V152, 2014.

[35] K. Nose-Filho, A. K. Takahata, R. Lopes, and J. M. Romano, "A fast algorithm for sparse multichannel blind deconvolution," *Geophysics*, vol. 81, no. 1, pp. V7–V16, 2015.

[36] E. Liu, N. Iqbal, J. H. McClellan, and A. A. Al-Shuhail, "Sparse blind deconvolution of seismic data via spectral projected-gradient," *IEEE Access*, vol. 7, pp. 23740–23751, 2019.

[37] E. Esser, T. Lin, R. Wang, and F. J. Herrmann, "A lifted l1/l2 constraint for sparse blind deconvolution," in *Proc. 77th EAGE Conf. and Exhib.*, 2015.

[38] E. Esser, T. T. Lin, F. J. Herrmann, and R. Wang, "Resolving scaling ambiguities with the $\ell 1/\ell 2$ norm in a blind deconvolution problem with feedback," in *Proc. IEEE 6th Int. Workshop Comput. Adv. Multi Sensor Adaptive Process.*, 2015, pp. 365–368.

[39] N. Kazemi, R. Shor, and K. Innanen, "Illumination compensation with seismic-while-drilling plus surface seismic imaging," in *Proc. 80th EAGE Conf. Exhib.*, 2018.

[40] N. Kazemi, E. Bongajum, and M. D. Sacchi, "Surface-consistent sparse multichannel blind deconvolution of seismic signals," *IEEE Trans. Geosci. Remote Sens.*, vol. 54, no. 6, pp. 3200–3207, Jun. 2016.

[41] G. Schuster, J. Yu, J. Sheng, and J. Rickett, "Interferometric/daylight seismic imaging," *Geophys. J. Int.*, vol. 157, no. 2, pp. 838–852, 2004.

[42] R. Snieder, "Extracting the greens function from the correlation of coda waves: A derivation based on stationary phase," *Phys. Rev. E*, vol. 69, no. 4, 2004, Art. no. 046610.

[43] N. M. Shapiro, M. Campillo, L. Stehly, and M. H. Ritzwoller, "High-resolution surface-wave tomography from ambient seismic noise," *Science*, vol. 307, no. 5715, pp. 1615–1618, 2005.

[44] K. Wapenaar, E. Slob, and R. Snieder, "Unified greens function retrieval by cross correlation," *Phys. Rev. Lett.*, vol. 97, no. 23, 2006, Art. no. 234301.

[45] A. Curtis, P. Gerstoft, H. Sato, R. Snieder, and K. Wapenaar, "Seismic interferometry turning noise into signal," *Leading Edge*, vol. 25, no. 9, pp. 1082–1092, 2006.

[46] G. T. Schuster, *Seismic Interferometry*, vol. 1. Cambridge, U.K.: Cambridge Univ. Press, 2009.

[47] K. Wapenaar and J. Fokkema, "Greens function representations for seismic interferometry," *Geophysics*, vol. 71, no. 4, pp. SI33–SI46, 2006.

[48] J. F. Claerbout, "Synthesis of a layered medium from its acoustic transmission response," *Geophysics*, vol. 33, no. 2, pp. 264–269, 1968.

[49] D. Draganov, K. Wapenaar, and J. Thorbecke, "Seismic interferometry: Reconstructing the earths reflection response," *Geophysics*, vol. 71, no. 4, pp. SI61–SI70, 2006.

[50] L. Borcea, G. Papanicolaou, and C. Tsogka, "Coherent interferometric imaging in clutter," *Geophysics*, vol. 71, no. 4, pp. SI165–SI175, 2006.

[51] L. Demanet and V. Jugnon, "Convex recovery from interferometric measurements," *IEEE Trans. Comput. Imag.*, vol. 3, no. 2, pp. 282–295, Jun. 2017.

[52] C. A. Vidal, D. Draganov, J. Van der Neut, G. Drijkoningen, and K. Wapenaar, "Retrieval of reflections from ambient noise using illumination diagnosis," *Geophys. J. Int.*, vol. 198, no. 3, pp. 1572–1584, 2014.

[53] C. Gradl, A. W. Eustes, and G. Thonhauser, "An analysis of noise characteristics of drill bits," *J. Energy Resources Technol.*, vol. 134, no. 1, 2012, Art. no. 013103.

[54] J. Rector III and B. P. Marion, "The use of drill-bit energy as a downhole seismic source," *Geophysics*, vol. 56, no. 5, pp. 628–634, 1991.

[55] B. Joyce, D. Patterson, J. Leggett, and V. Dubinsky, "Introduction of a new omni-directional acoustic system for improved real-time LWD sonic logging-tool design and field test results," in, *SPWLA 42nd Annual Logging Symposium*. Houston, TX, USA: Soc. of Petrophysicists and Well-Log Analysts, 2001.

[56] I. Vasconcelos and R. Snieder, "Interferometry by deconvolution: Part 1theory for acoustic waves and numerical examples," *Geophysics*, vol. 73, no. 3, pp. S115–S128, 2008.

[57] R. Snieder and E. Safak, "Extracting the building response using seismic interferometry: Theory and application to the millikan library in pasadena, california," *Bulletin Seismological Soc. America*, vol. 96, no. 2, pp. 586–598, 2006.

[58] K. Wapenaar, J. van der Neut, and E. Ruigrok, "Passive seismic interferometry by multidimensional deconvolution," *Geophysics*, vol. 73, no. 6, pp. A51–A56, 2008.

[59] K. Wapenaar *et al.*, "Seismic interferometry by crosscorrelation and by multidimensional deconvolution: A systematic comparison," *Geophys. J. Int.*, vol. 185, no. 3, pp. 1335–1364, 2011.

[60] J. van der Neut, J. Thorbecke, K. Mehta, E. Slob, and K. Wapenaar, "Controlled-source interferometric redatuming by crosscorrelation and multidimensional deconvolution in elastic media," *Geophysics*, vol. 76, no. 4, pp. SA63–SA76, 2011.

[61] F. Broggini, R. Snieder, and K. Wapenaar, "Data-driven wavefield focusing and imaging with multidimensional deconvolution: Numerical examples for reflection data with internal multiples," *Geophysics*, vol. 79, no. 3, pp. WA107–WA115, 2014.

[62] S. Makino, H. Sawada, R. Mukai, and S. Araki, "Blind source separation of convolutive mixtures of speech in frequency domain," *IEICE Trans. Fundamentals Electron., Commun. Comput. Sci.*, vol. 88, no. 7, pp. 1640–1655, 2005.

[63] P. Bharadwaj, L. Demanet, and A. Fournier, "Deblending random seismic sources via independent component analysis," in, *SEG Tech. Program Expanded Abstracts*. Tulsa, OK, USA: Soc. of Exploration Geophysicists, 2017.

[64] G. Ayers and J. C. Dainty, "Iterative blind deconvolution method and its applications," *Opt. Lett.*, vol. 13, no. 7, pp. 547–549, 1988.

[65] F. Sroubek and P. Milanfar, "Robust multichannel blind deconvolution via fast alternating minimization," *IEEE Trans. Image Process.*, vol. 21, no. 4, pp. 1687–1700, Apr. 2012.

[66] J. Dolloff, B. Lofy, A. Sussman, and C. Taylor, "Strictly positive definite correlation functions," *Proc. SPIE*, vol. 6235, 2006, p. 62351A.

[67] L. Vandenberghe and S. Boyd, "Semidefinite programming," *SIAM review*, vol. 38, no. 1, pp. 49–95, 1996.

[68] M. R. Osborne, B. Presnell, and B. A. Turlach, "A new approach to variable selection in least squares problems," *IMA J. Numer. Anal.*, vol. 20, no. 3, pp. 389–403, 2000.

[69] J. Bezanson, A. Edelman, S. Karpinski, and V. B. Shah, "Julia: A fresh approach to numerical computing," *SIAM Rev.*, vol. 59, no. 1, pp. 65–98, 2017.

[70] P. Bharadwaj. A Julia package for multichannel blind deconvolution with focusing constraints, 2018. [Online.] Available: https://github.com/pawbz/FocusedBlindDecon.jl.git

[71] D. C.-L. Fong and M. Saunders, "LSMR: An iterative algorithm for sparse least-squares problems," *SIAM J. Sci. Comput.*, vol. 33, no. 5, pp. 2950–2971, 2011.

[72] P. K. Mogensen and A. N. Riseth, "Optim: A mathematical optimization package for Julia," *J. Open Source Softw.*, vol. 3, no. 24, p. 615, 2018. [Online]. Available: https://juliaobserver.com/packages/Optim

[73] A. Brougois, M. Bourget, P. Lailly, M. Poulet, P. Ricarte, and R. Versteeg, "Marmousi, model and data," in *Proc. EAEG Workshop-Practical Aspects Seismic Data Inversion*, 1990.

Laurent Demanet received Undergraduate degree in mathematical engineering and theoretical physics from Universite de Louvain, Ottignies-Louvain-la-Neuve, Belgium, and the Ph.D. degree in 2006 under Emmanuel Candes, in applied and computational mathematics from Caltech, Pasadena, CA, USA. He is currently a Professor of applied mathematics with the Department of Mathematics, MIT, Cambridge, MA, USA. He is also the Director of MIT's Earth Resources Laboratory. Previously, he held a postdoctoral position called "Szego Assistant Professor" with the Department of Mathematics at Stanford. His research interests include signal processing, inverse problems, and wave propagation. He is the recipient of a Sloan research fellowship, a CAREER award from NSF, and a Young Investigator award from AFOSR.

Pawan Bharadwaj received the Master of Science degree in geophysics from Indian Institute of Technology (Indian School of Mines), Dhanbad, India, and the Ph.D. degree in geophysics from Delft University of Technology, Delft, The Netherlands, in 2016. He is currently a Postdoctoral Associate with a joint appointment with the Department of Mathematics and Earth Resources Laboratory, MIT, Cambridge, MA, USA. His expertise is in inverse problems and signal processing relevant to seismic wave propagation and scattering.

Aimé Fournier received the Ph.D. degree in physics from Yale University, New Haven, CT, USA, in 1997. He was a Research Associate with the Department of Atmospheric and Oceanic Science, University of Maryland, College Park (1998–1999), an Advanced Study Program Fellow and Project Scientist with the National Center for Atmospheric Research (2000–2010), and a Senior Research Geophysicist with the Schlumberger (2011–2014). Since 2015, he has been a Research Scientist and Principal Investigator with the Earth Resources Laboratory, Department of Earth, Atmospheric and Planetary Sciences, Massachusetts Institute of Technology, and a Research Associate Professor with the Department of Mathematical and Statistical Sciences, University of Colorado Denver.